Mobile Radar and Fixed-Location Radar Data Comparison for a VORTEX2 Case: Two Tornadic Supercells on May 19, 2010

Christopher M. Schwarz and Donald W. Burgess*
Cooperative Institute for Mesoscale Meteorological Studies, The University of Oklahoma, Norman, OK

1. INTRODUCTION

On 19 May 2010, two tornadic supercells occurred across north-central Oklahoma. The storms were within the unambiguous range of two fixed S-band (10-cm wavelength) radars, the Multi-function Phased Array Radar (MPAR, referred to hereafter as PAR; e.g., Heinselman et al. 2008; Weadon et al. 2009), and the Twin Lakes Weather Surveillance Radar - 1988 Doppler (KTLX; WSR-88D). In addition, these tornadic supercells were primary targets of The Verification of the Origins of Rotation in Tornadoes Experiment 2 (VORTEX2; Wurman et al. 2012) field campaign. One of the mobile radars from VORTEX2 (hereafter simply V2), the NOAA X-band (3-cm wavelength) dual-Polarized mobile radar (NOXP; Burgess et al. 2010), was able to simultaneously sample both supercells. Since three different radars adequately sampled both storms, this provided an opportunity to compare the differences in spatial and temporal resolution between the PAR and an operational WSR-88D, and a mobile research radar (NOXP). The purpose of this paper is to provide advantages and disadvantages of the PAR and WSR-88D when compared to high-resolution mobile radar data. Section 2 of this paper briefly discusses background of the radars; Section 3 gives the technical specifications of the radars, and Section 4 provides information on data preparation. Section 5 illustrates and discusses the radar comparisons, Section 6 will detail the time evolution of the mesocyclone shear signatures and the tornadic vortex signatures (TVSs), and Section 7 summarizes the paper.

*corresponding author address: Don Burgess, National Weather Center, 120 David L. Born Blvd., Norman, OK 73072
Email: Donald.Burgess@noaa.gov

2. BACKGROUND

a. Weather Surveillance Radar – 1988 Doppler (WSR-88D)

The Next-Generation Weather Radar (NEXRAD) network of WSR-88D radars was developed in the 1980s (Serafin and Wilson 2000). Over 160 S-band radars are in operation today, and are used by operational and research meteorologists daily. In 2008, the introduction of "super-resolution" (azimuthal oversampling every 0.5°, 0.25 km gate spacing, and 0.4° elevation oversampling) at all elevation scans below 1.6°, was utilized to help refine spatial detail in weather echoes. Legacy resolution (1° azimuthal sampling x 1 km gate spacing for Reflectivity and 1° azimuthal sampling x 250 m gate spacing for Radial Velocity) is still used for all higher elevation angles. Furthermore, super-resolution data extended the Radial Velocity coverage range to 300 km(http://www.roc.noaa.gov/wsr88d/buildinfo/build10faq.aspx#q1). However, super-resolution does not improve scan times during Volume Coverage Patterns (VCPs). Improved temporal resolution from the NEXRAD network has been desired for over a decade. Improving update times of radar data collection has been a focus of the National Weather Radar Testbed (NWRT; Forsyth et al. 2007) for the past five years.

b. Phased Array Radar

In the early 2000s, phased array technology was deemed a plausible candidate to "replace America's aging fleet of weather surveillance radars" (National Academies 2002). The PAR was designed as a multifunction system to provide radar support to both aviation and meteorologists simultaneously (e.g., Weber et al. 2007; Zrnic et al. 2007; Heinselman et al. 2008). The principle ideas of lowering maintenance costs of the aging WSR-88Ds, and the enhancement of temporal resolution (<1-2 minute full volumes compared to 4.25-5 minute full volumes for the WSR-88Ds) during severe weather were two driving forces for the PAR system (Weadon et al. 2009). With the enhancement of temporal resolution, the added amount of data could provide severe weather and aviation forecasters better information for improved weather warnings. A report from the Office of the Federal Coordinator for Meteorology (OFCM) laid out a research and development plan of action to build a full S-band PAR prototype to answer logistical questions before a final acquisition decision would be made (Weadon et al. 2009).

The NWRT PAR, the radar in this study, is used in research and operational testing in Norman, OK. It is not designed to achieve operational-like performance or to serve as a prototype for the multi-function phased array radar (MPAR), but to demonstrate the operational utility of some of the unique capabilities offered by PAR technology that may eventually drive the design of future operational weather radars (Heinselman and Torres 2011).

c. NOAA X-band Polarized Mobile Radar

NOXP was built on a flatbed International Truck frame by Alan Zahrai and his group of NSSL engineers and technicians in 2008 (Palmer et al. 2009). This radar was used during both years of V2 (2009 and 2010) as one of four mesocyclone-scale radars (i.e. a radar that deployed between 10 and 30 km range from the target storm). The close range allowed higher resolution observations of low- and mid-level mesocyclones in supercells. Furthermore, although not used in this study, NOXP has polarization diversity capability.

3. TECHNICAL SPECIFICATIONS

a. Scanning Strategies

As part of PAR testing and research, the NWRT group emulates conventional VCPs of operation WSR-88Ds during precipitation episodes. Typically, similar PAR elevation angles and number of samples are chosen to match WSR-88D modes.

On 19 May 2010, PAR utilized a combination of strategies termed "Oversampled VCP within 120 km only" and "Tornadic within 120 km only", which consists of twenty-two tilts and a VCP update time of 1.4 minutes, and four low-level tilts prior to twenty-two tilts with a combined VCP update time of 2.3 minutes, respectively. The latter is interlaced within the collection of every other scan. This provides a significant advantage over the 4.25 minute VCP 12 scan strategy of KTLX for severe convection; more scans in a shorter period of time. However, the current PAR in Norman has only one flat-panel array face. That panel is mounted onto a moving pedestal to rotate the antenna. This limits the region of observation to a 90° sector in the direction the face is pointing. It should be noted that if Phased Array Radar goes into operation, it would contain as many as four array faces (Heinselman et al. 2008, Brown and Wodd, 2013). For more information on the PAR, the reader is deferred to the studies of Weber et al. 2007, Zrnic et al. 2007, Heinselman et al. 2008, and Heinselman and Torres 2011.

WSR-88D VCP 12 with super-resolution has an update time of 4.25 minutes, and consists of fourteen elevation angles in a full volume scan. The low-level (<1.6°) elevations are split-cut scans, i.e., two scans are collected at each low-level elevation; one for Reflectivity and one for Radial Velocity estimates. The lowest three elevation angles consist of the super-resolution scans. Split cuts for low elevations angles are also a part of PAR scanning.

NOXP used full 360° PPI scans as the primary scanning strategy in 2010. Certain limitations restricted the radar's antenna rotation rate to 29°/sec. At this rate, combined with a full 360° scan, NOXP's data volumes were restricted to 7° in elevation angle for 2-minute time syncs with other V2 radars. This low upper-angle limit prevented the radar from topping storms close to the radar. Table 1 details the technical specifications of the three radars. Table 2 details the scanning strategies of the three radars.

Radar Name	PAR	KTLX	NOXP
Wavelength	S-band (λ=10-cm)	S-band (λ=10-cm)	X-band (λ=3.21 cm)
Frequency	~2700-~3000 MHz	~2700-~2900 MHz	9410 MHz
3-dB Beamwidth	1.5° boresight/ 2° at edges of sector	0.93° (at 2850 MHz, Measured Average)	0.95°
Az. Sampling	~0.8° boresight / ~1° at edges of sector	0.5° (super-res.) / 1° (legacy res.)	0.5°
Nyquist- Co-Interval	28.15 m/s	26.12 m/s	19.9 m/s
Gate Length	0.24 km	0.25 km (super-res.) / 1 km (Ref. - legacy res.) 0.25 km (Rad. Vel. – legacy res.)	0.075 km
Max Unambiguous Range	420.4 km	460 km (Ref.) 300 km (Rad. Vel. – super res.) / 230 km (Rad. Vel. – legacy res.)	59 km
Peak Power	750 kW	750 kW	250 kW

Table 1 – Technical specifications for the PAR, KTLX, and the NOXP mobile radar during the 2010 data collection season.

Radar Name	PAR	KTLX	NOXP
Beam Steering	Mechanically Rotating Pedestal w/ Electronic Beam Steering	Mechanically Rotating Pedestal w/ Elevation Drive	Mechanically Rotating Pedestal w/ Elevation Drive
Sectors Collected	90°	360°	360°
Elevations Collected	0.51°, 0.81°. 1.15°, 1.54°, 1.98°, 2.48°, 3.07°, 3.75°, 4.54°, 5.48°, 6.59°, 7.9°, 9.46°, 11.32°, 13.55°, 16.22°, 19.45°, 23.37°, 28.2°, 34.25°, 42.08°, 52.9°	0.5°, 0.9°, 1.3°, 1.8°, 2.4°, 3.1°, 4.0°, 5.1°, 6.4°, 8.0°, 10.0°, 12.5°, 15.6°, 19.5°	1.0°, 2.0°, 3.0°, 4.0°, 5.0°, 6.0°, 7.0°

Table 2 – The scanning strategies for the PAR, KTLX, and the NOXP mobile radar during the 2010 data collection season.

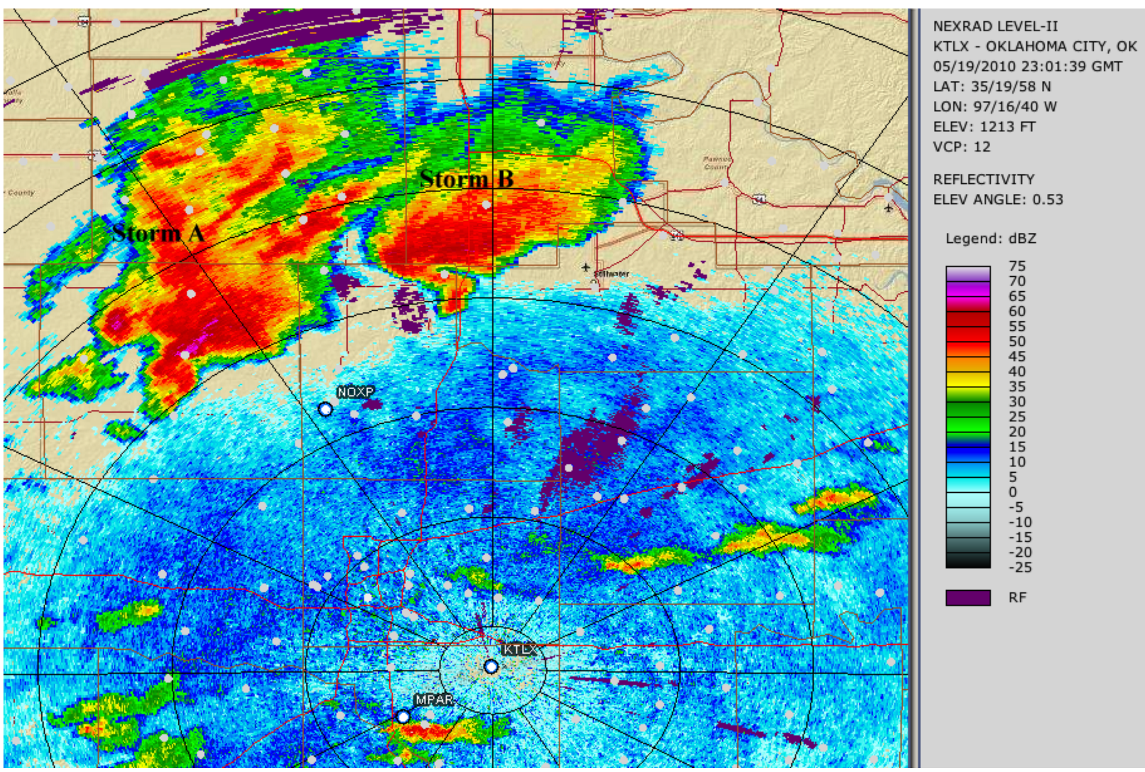

Figure 1 – Reflectivity from the KTLX 0.5° elevation scan at 2301:39 UTC. Locations of NOXP, PAR (denoted as MPAR), and KTLX are marked on the image. Also "Storm A" and "Storm B" are denoted as the two storms of interest in this study. Image from NCDC Weather and Climate Toolkit.

4. DATA PREPARATION

Both KTLX and PAR data were converted from their native message 31 formats to DORADE Sweep format for editing in SOLOII (Oye et al. 1995). The data were de-aliased and ground clutter was removed. Similarly, the NOXP data were converted from RAW Sigmet format to DORADE Sweep format to be de-aliased and have ground clutter removed. Using the Matplotlib library in Python v. 2.7, Plan Position Indicator (PPI) plots were created to illustrate the various elevation scans of the three radars. All beam height calculations are estimated using the following equation from Doviak and Zrnic (1993):

$$h = [r^2 + (\frac{4}{3}a)^2 + 2r(\frac{4}{3}a)\sin\theta_e]^{\frac{1}{2}} - (\frac{4}{3}a)$$

where a is the radius of the earth, r is the range to the target, and θ_e is the elevation angle at which the radar is scanning. The processing procedures resulted in missing sections of data in Radial Velocity where range folding (purple haze) resided in the PAR and WSR-88D data.

5. DATA COMPARISON AND ANALYSIS

During the events of 19 May 2010, all three radars used in this study sampled two tornadic storms simultaneously. The first storm produced an EF1 tornado near Kingfisher, OK (Storm A). The second storm produced an EF0 tornado near Orlando and an EF1 tornado near Lake Carl Blackwell (Storm B). Fig. 1 shows the location of the three radars and Storms A and B. Due to earth's curvature and the distances of the radar to a tornadic storm, the most vital information to meteorologists during events of severe weather events may lie within the few lowest few elevation scans. Therefore, most emphasis will be on the lowest four elevation scans of the farther-range radars (KTLX and PAR).

Radar Name	PAR	KTLX	NOXP
Mean Range: Tornadic Storm 1	89.5 km	86.5 km	25.5 km
Mean Range: Tornadic Storm 2	98.5 km	90 km	38 km
Elevation Angle - Beam Height ARL (@ Mean Range for Tornadic Storm 1)	0.51°-1.27 km, 0.81°-1.74 km, 1.15°-2.27 km, 1.54°-2.88 km, 1.98°-3.56 km, 2.48°-4.34 km, 3.07°-5.26 km, 3.75°-6.32 km, 4.55°-7.6 km, 5.48 °-9.02 km, 6.59°-10.74 km, 7.9°-12.76 km	0.5°-1.19 km, 0.9°-1.80 km, 1.3°-2.40 km, 1.8°-3.16 km, 2.3°-4.06 km, 3.1°-5.12 km, 4.0°-6.47 km, 5.1°-8.12 km, 6.4°-10.08 km, 8.0°-12.47 km,	1.0°-0.48 km, 2.0°-0.93 km, 3.0°-1.37 km, 4.0°-1.82 km, 5.0°-2.26 km, 6.0°-2.70 km, 7.0°-3.14 km
Elevation Angle / Beam Height ARL (@ Mean Range for Tornadic Storm 2)	0.51°-1.44 km, 0.81°-1.96 km, 1.15°-2.55 km, 1.54°-3.22 km, 1.98°-3.97 km, 2.48°-4.83 km, 3.07°-5.84 km, 3.75°-7.01 km, 4.54°-8.36 km, 5.48°-9.97 km, 6.59°-11.87 km, 7.9°-14.10 km	0.5°-1.26 km, 0.9°-1.89 km, 1.3°-2.52 km, 1.8°-3.03 km, 2.3°-4.24 km, 3.1°-5.34 km, 4.0°-6.75 km, 5.1°-8.47 km, 6.4°-10.5 km, 8.0°-12.99 km	1.0°-0.75 km, 2.0°-1.41 km, 3.0°-2.07 km, 4.0°-2.74 km, 5.0°-3.40 km, 6.0°-4.06 km, 7.0°-4.71 km

Table 3 – The beam heights above radar level (ARL) of all three radars used in this study. The beam heights are estimated at a mean range to each tornado.

Table 3 indicates the beam height above radar level (ARL) for all three radars at their respective mean ranges for both tornadoes. Given the closer proximity of NOXP to the target storms, the higher elevation angles (3°-7°) are primarily used in the comparison, to give the closest equivalent beam height to the lower elevation angles for the PAR and KTLX.

NOXP's deployment began at 2300 and lasted until 2336 UTC; all times hereafter are UTC). All emphasis for Storm A comparison will be near the beginning of the deployment to include the latter stages of the Kingfisher tornado, which lasted from 2245 until 2309. Storm B's comparisons will be split between the Orlando tornado (2303-2311) and the Lake Carl Blackwell tornado (2314-2338).

a. Spatial Resolution Comparisons

Since NOXP began scanning at ~2300, the closest time of a KTLX 4.25-minute VCP was ~2301, and could be paired with a PAR VCP that began at ~2301. Figs 2 and 3 (Storm A and B, respectively) indicate the differences in spatial resolution between the three radars at nearly equal height, using the 0.5° elevation for KTLX and PAR and the 3.0° elevation for NOXP; all beam heights matched at ~1.5 km ARL height. The middle panels are examples of what an operational forecast meteorologist would currently see in terms of resolving the echo at low-levels.

In the top panel, the wider beam width of the PAR results in less spatial resolution, compared to the other two radars. Keep in mind that both KTLX and PAR are azimuthally oversampling, but the PAR beam width is still somewhat larger. This is particularly evident in Radial Velocity around the region of the mesocyclone (x=-59, y=67; in middle panel of Fig. 2). The larger sample area, a result of the wider beam width, negatively impacts the estimates at each radar range gate in the PAR data compared to the other two radars. This limitation of spatial resolution restricts the capability to accurately resolve the tornado signature in velocity. NOXP, however, has the advantage of being mobile which allows it to move closer to the target. This capability helps reduce the effects of resolution degradation from a widening beam due to increasing range. The NOXP details in and around the hook echo allow the user to resolve smaller scale features, i.e., the Kingfisher mesocyclone/TVS signature at x=-26, y=8, and the separate strong RFD wind max at x=30, y=7, both in the bottom panel of Fig. 2. Neither KTLX nor PAR can clearly resolve the two different signatures. Furthermore, NOXP can better resolve the hook echo and weak echo region (WER), both trademarks of supercell thunderstorms. The same is true for the insipient Orlando tornado in Fig. 3 where neither KTLX or PAR can resolve the details of the mesocyclone, hook, or WER, i.e. near x=25, y=30, bottom panel. Similar spatial resolution comparisons can be seen in Figs. 4 and 5 for somewhat higher heights within the storms (~ 3 km ARL height).

NOXP is X-band, which, unfortunately, means attenuation is problematic, i.e., signal loss due to absorption and scattering due to the shorter wavelength. In Figs. 2 - 5, the extinction of signal is evident (note the missing echo behind the core for NOXP when compared to KTLX and PAR). This is a major drawback for X-band radars and a major reason for the use of S-band radars for operational meteorology.

Figs. 2 and 3 also illustrate the goodness of super-resolution data from the WSR-88Ds. However, above the 1.5° elevation scan, the scanning strategy switches to legacy resolution as seen in Figs. 4 and 5. While Radial Velocity data suffer some resolution reduction, there is remarkable degradation of resolution in Reflectivity, making identification of characteristics of each supercell increasingly difficult. It is at these levels, where the PAR obtains some advantage in Reflectivity spatial resolution.

Examining the PAR's Radial Velocity field on the eastern edge of the echo in Fig. 5, there is suggestion that there might be some impacts of horizontal and/or vertical side lobe issues. As shown in Fig. 6, this is identified in the region of strong outbound radial velocities on the eastern flanks the hook echo, WER and echo overhang region, which is not apparent at the closest coincident elevation in KTLX (PAR's beam is at 2.88 km AGL and KTLX's beam is at 3.16 km AGL). These strong outbound radial velocities are not observed until the 2.3° and 3.1° elevations in KTLX, implying vertical side-lobe contribution. This obviously can have adverse effects for meteorological forecasters. The times between the PAR and KTLX are within 23 seconds of each other for the corresponding heights. It is unlikely to have such drastic evolution of the wind field during such a small time change. For Storm B around 2323, this side lobe issue is apparent throughout the low-level velocity scans as shown in Fig. 7. In comparing KTLX to PAR, the annotated blue circle on the right side of the KTLX and PAR images indicates a region of strong cyclonic shear. However, the widening beam width near the edge of the PAR's sector (approaching 2°) and side lobes inhibit its ability to adequately resolve the vortex signature.

b. Temporal Resolution Comparisons

A few studies have previously utilized the high temporal resolution of the PAR for studies of severe weather (e.g., Heinselman et al. 2008; Newman and Heinselman, 2012). The PAR's capability to rapidly collect volumes of data is extremely useful for tornadic supercells. For the current data set, for every volume of 88D data, PAR, on average, collected 2.5 VCPs. This is obviously advantageous for research meteorologists, but especially advantageous for operational forecasters due to the quantity of information being returned (Heinselman *et al*, 2012). What the PAR lacks in low-level spatial resolution, it makes up for with temporal resolution. In the case of the Kingfisher tornado, NOXP sampled the tornado for ~9 minutes. This equates to roughly four full volume scans from the PAR (remember that a few sets of four low-level [0.51-1.54°] were interlaced into the scans), compared to two volumes of the WSR-88D. A lot of valuable information on the evolution of the storm and the tornado is missed between volumetric updates on the 88D.

Fig. 7 illustrates a prime situation where the rapid volumetric updates would benefit operational meteorological forecasters in the event of tornado warning decisions. Annotated in the figure are two regions of interest in both the PAR and KTLX for Storm B at ~2323. One shear region (to the northwest) is with the Lake Carl Blackwell tornado; the other shear region (to the southeast) is with a newly developing mesocyclone (part of the storm cyclic process) that did not go on to eventually produce a tornado. Strong rotation is observed through the lowest four tilts. The annotated shear signature on the upper left coincides with a confirmed tornado. However, the forecaster would also want to have as much information as possible on the new, rapidly developing circulation.

6. TIME TRENDS OF TVS AND MESOCYCLONE SHEAR

Plots of low-level (0.5^{o} elevation angle) mesocyclone differential velocity (DV) versus time for the three mesocyclones are shown in Figs. 8-10. Data are only available for the weakening stages of the Kingfisher and Orlando mesocyclones, but are available for much of the lifetime of the Lake Carl Blackwell mesocyclone. Surprisingly, for the Kingfisher mesocyclone (Fig. 8), both PAR and KTLX have larger DVs than NOXP. Likely, this results from the wider beam widths of the longer-range radars mixing together the low-level mesocyclone and RFD wind signature that the closer-range NOXP was able to resolve as separate features. Note that the increased number of PAR scans reveals small-scale DV changes missed by KTLX.

The plot for the Orlando mesocyclone (Fig. 9) is different from that of the Kingfisher mesocyclone, and contains the more expected result of biggest DVs with the highest-spatial-resolution radar (NOXP) and the smallest DVs with lowest-spatial-resolution radar (PAR).

The longer plot for the Lake Carl Blackwell mesocyclone plot (Fig. 10) is different from the previous two in that NOXP and PAR DVs are similar, while KTLX DVs are smaller and without significant trends. The similarity of the NOXP and PAR plots likely results from the PAR side-lobe vertical contamination that allowed velocities from higher heights to incorrectly be shown on the lower elevation angle. Even with the addition of the side-lobe contamination, the ability of the PAR to capture higher temporal trends in mesocyclone strength is impressive.

The three tornadoes produced by storms A and B were all weak (EF0-1). However, using a modest threshold to detect TVSs (30 m/s DV with diameter <1 km), the nearby radar (NOXP) detected TVSs for all three for all scans during the portion of their lifetimes that were during the study period. As might be expected from sampling considerations, the farther-range radars (PAR and KTLX) did not detect the TVSs as often (Fig. 11), including the few scans where the TVS was somewhat stronger (DV >45 m/s).

7. SUMMARY

The National Weather Radar Testbed Phased Array Radar's (PARs) spatial and temporal resolution is compared to the Twin Lakes Weather Surveillance Radar – 1988 Doppler (KTLX WSR-88D) and the NOAA X-band Polarized (NOXP) mobile radar for two tornadic supercells on 19 May 2010. In this study the PAR's scanning strategies mimic the scanning strategy of the Volume Coverage Pattern 12 (VCP 12) that the National Weather Service (NWS) utilizes for severe convection. NOXP's near-range, high-resolution data are used as ground truth to compare PAR and KTLX data. It is shown that at low elevation angles, the PAR has a disadvantage in terms of spatial resolution. KTLX's narrower beam width (~1.0°), compared to PAR's 1.5° at boresight, and up to 2.0° off boresight, helps it better depict storm details. In comparing the two, the 88D's "super-resolution" scans (lowest three elevation angles) gain the most advantage in terms of spatial resolution. However, above 1.6° in elevation, the 88D switches to legacy resolution scans (1° x 1 km resolution for Reflectivity and 1° x 250 m for Radial Velocity). Here, the PAR has some advantage in terms of Reflectivity spatial resolution.

The WSR-88Ds have a mechanically rotated antenna, resulting in 4.25 minute VCPs. For this study, PAR is capable of completing a full volume scan in 1.4 minutes [In other studies, PAR updates have been even faster; less than 1 minute.] Much temporal information about storm evolution is lost to meteorological forecasters when WSR-88D data are compared to PAR data.

For certain scans during the study, those near the WER with echo overhang above, PAR appears to be suffering from side lobe contamination. This study suggests that PAR may have side lobe issues, particularly apparent well off boresight, that need further investigation for minimization in prototype development.

Acknowledgements:

The authors wish to thank Gordon Carrie, Arthur Witt, Jeff Brogden, and Kevin Manross for their help with processing both the PAR data and the WSR-88D data. They also wish to thank Pam Heinselman for the information provided concerning the 2010 Phased Array Radar scanning strategies. This work is funded by NOAA/Office of

Oceanic and Atmospheric Research under NOAA-University of Oklahoma Cooperative Agreement #NA11OAR430072. Funding for NOXP VORTEX2 research came from NSF ATM-0802717.

REFERENCES

Brown, R.A., and V.T. Wood, 2013: Simulated vortex detection using a four-face array Doppler radar. *Wea. Forecasting*, in press.

Doviak, R. J., and D. S. Zrnic, 1993: *Doppler Radar and Weather Observations.* Academic Press, 562 pp.

Heinselman, P. L., D. L. Priegnitz, K. L. Manross, T. M. Smith, R.W. Adams, 2008: Rapid sampling of severe storms by the national weather radar testbed phased array radar. *Wea. Forecasting*, **23**, 808–824.

______, and S. M. Torres, 2011: High-temporal-resolution capabilities of the National Weather Radar Testbed phased-array radar. *J. of Appl. Meteor. and Climate*., **50,** 579-593.

______, D.S. Ladue, and H. Lazurus, 2012: Exploring impacts of rapid-scan radar data on NWS warning decisions. *Wea. Forecasting*, **27**, 1031-1044.

National Academies, 2002: Weather Radar Technology Beyond NEXRAD. National Research Council, National Academy of Science, National Press Tech. Rep., 96 pp.

Newman, J.F., and P.L. Heinselman, 2012: Evolution of a quasi-linear convective system sampled by a phased array radar. *Mon. Wea. Rev.*, **140**, 3467-3486.

Oye, R., C. K. Mueller, and S. Smith, 1995: Software for radar translation, visualization, editing, and interpolation. Preprints, *27th Conference on Radar Meteorology*, Vail, CO, American Meteorological Society, 359-361

Palmer, R., M. Biggerstaff, P. Chilson, G. Zhang, M. Yeary, J. Crain, Tian-You Yu, Y. Zhang, K. Droegemeier, Y. Hong, A. Ryzhkov, T. Schuur, and S. Torres, 2009: Weather radar education at the University of Oklahoma-an integrated interdisciplinary approach. *Bull. Amer. Meteor. Soc.*, **90,** 1277-1282.

Serafin, R. J., and J. W. Wilson, 2000: Operational weather radar in the United States: Progress and opportunity. *Bull. Amer. Meteor. Soc.*, **81,** 501-518.

Weadon, M., P. L. Heinselman, D. Forsyth, J. Kimpel, W. E. Benner, G. S. Torok, 2009: Multifunction phased array radar. *Bull. Amer. Meteor. Soc.*, **90**, 385–389.

Weber, M., J. Y. N. Cho, J. S. Flavin, J. M. Herd, W. Benner, and G. Torok, 2007: The next-generation multimission U.S. surveillance radar network. *Bull. Amer. Meteor. Soc.*, **88,** 1739-1751.

WSR-88D Build 10/Super Resolution Level II FAQs Updated 19 October 2007. U.S. Dept. of Commerce, National Oceanic and Atmospheric Administration, National Weather Service, Radar Operations Center (website owner) URL:[http://www.roc.noaa.gov/wsr88d/buildinfo/build10faq.aspx#q1]

Wurman, J., D. Dowell, Y. Richardson, P. Markowski, E. Rasmussen, D. Burgess, L. Wicker, and H. Bluestein, 2012: Verification of the Origins of Rotation in Tornadoes Experiment 2: VORTEX. Submitted to *Bull. Amer. Meteor. Soc.*

Zrnic, D. S., and Coauthors, 2007: Agile-beam phased array radar for weather observations. *Bull. Amer. Meteor. Soc.*, **88**, 1753–1766.

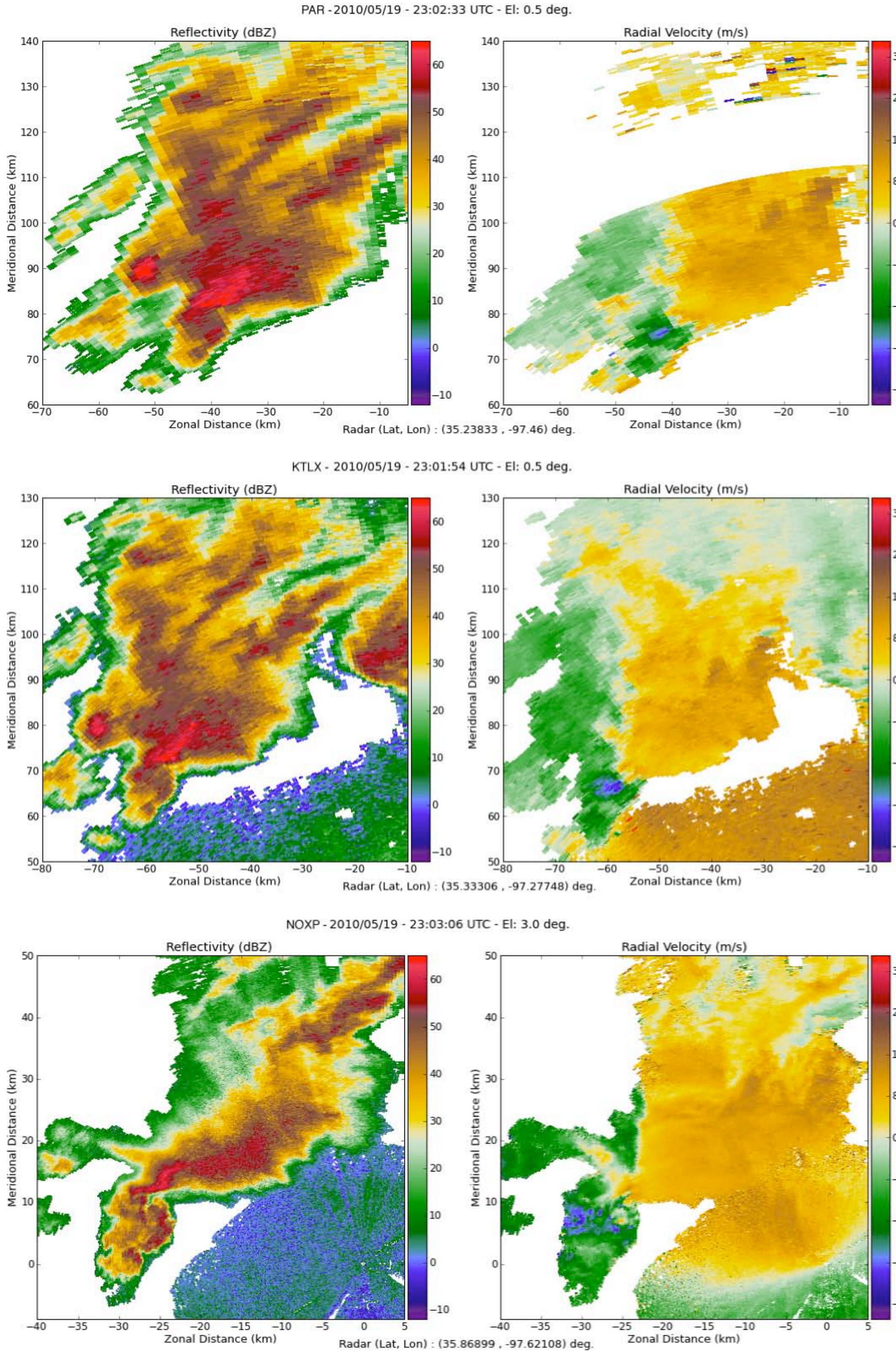

Figure 2 - Radar reflectivity factor (left side) and radial velocity (right side) from PAR (top), KTLX (middle), and NOXP (bottom) for Storm A. All elevations have coinciding beam heights. This set of image demonstrates the variation in the spatial resolution between the three radars at the highest available spatial resolution for each.

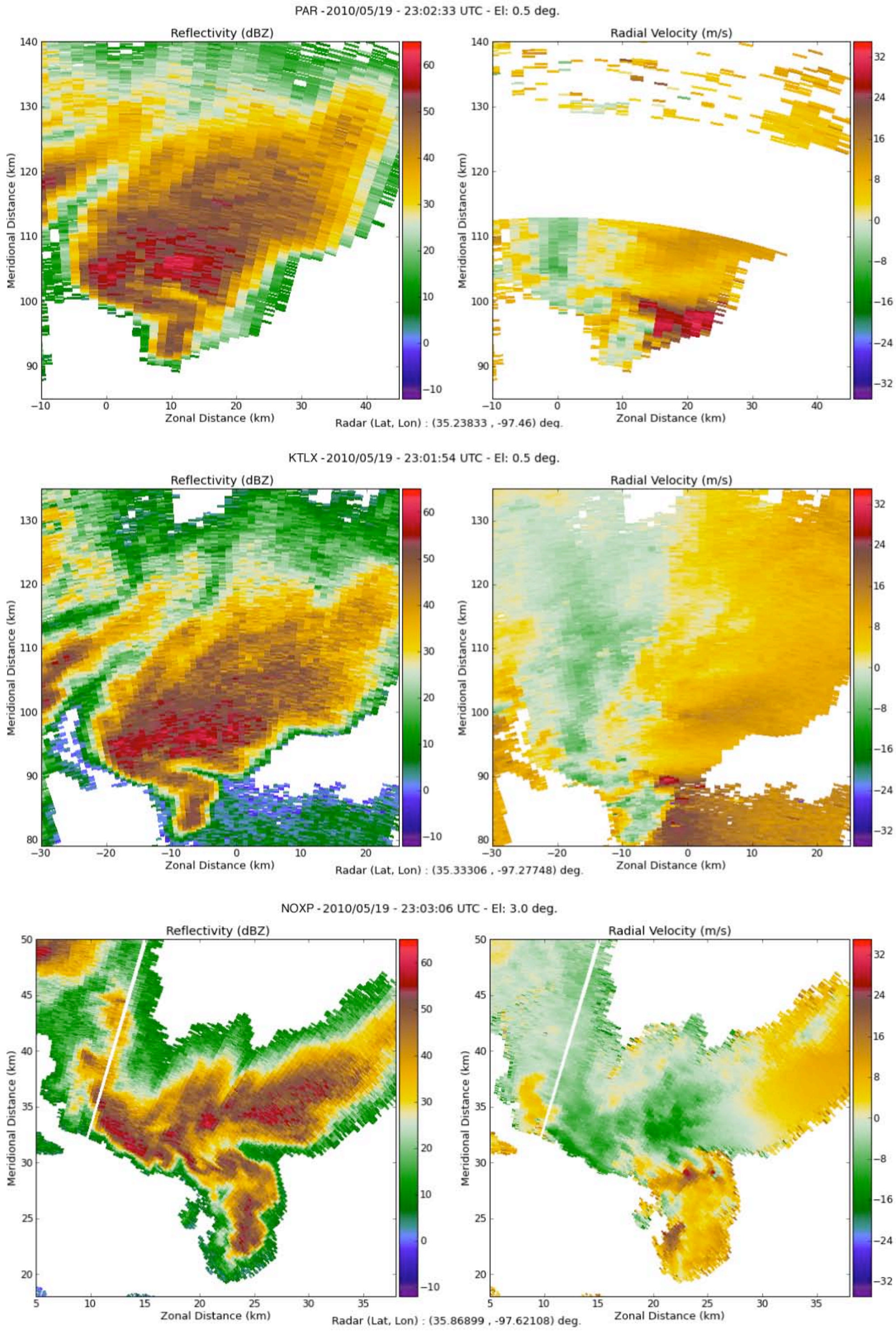

Figure 3 – Same as Fig. 2 but for Storm B. Note the substantial amount of attenuation for NOXP. The loss of signal is very rapid through the precipitation core, while KTLX and PAR are able to sample the entire storm.

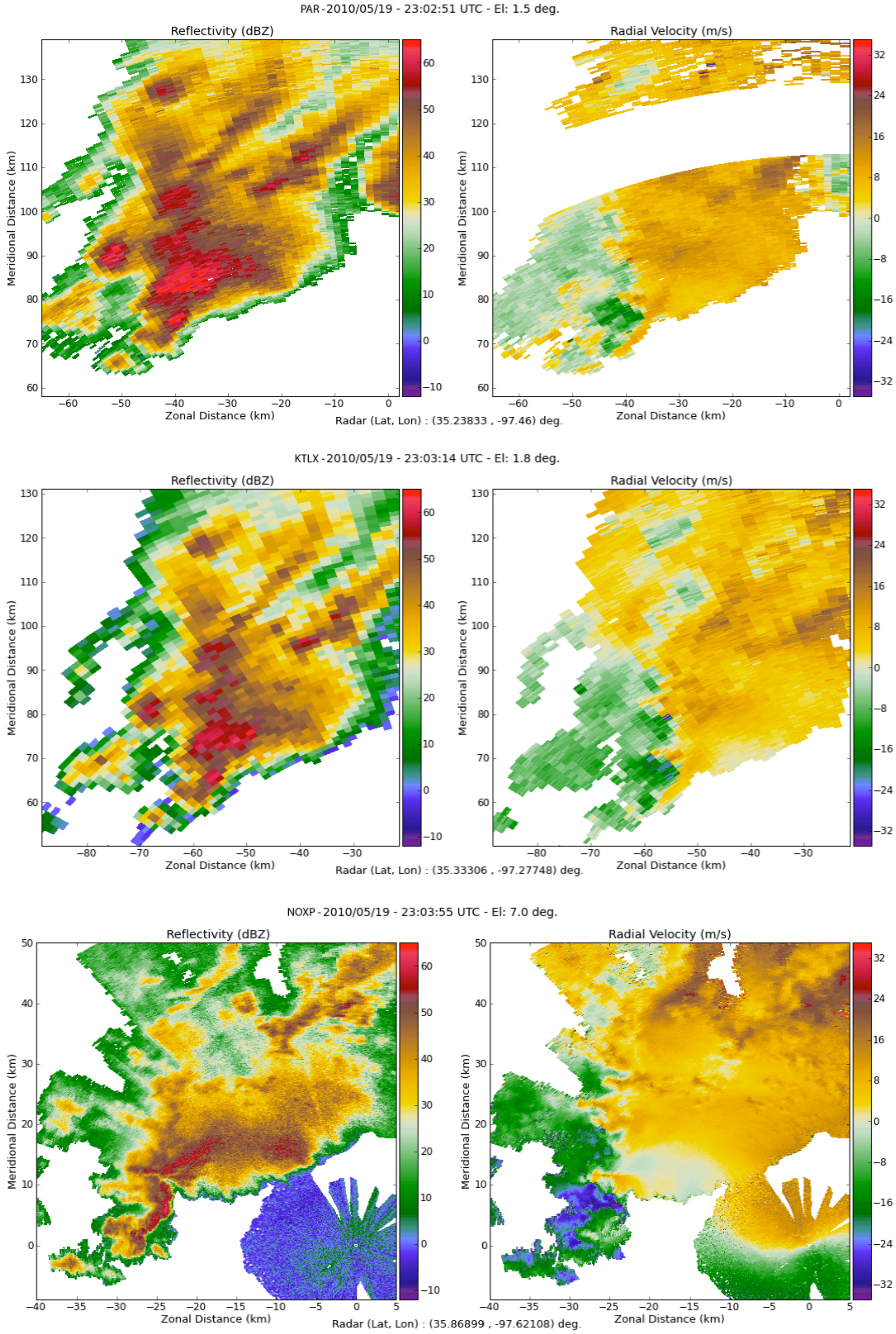

Figure 4 – Same configuration as Fig 2 but at KTLX's 1.8° elevation. Note the reduction of spatial resolution, as known as "legacy resolution", in the 88D data. The other two radars spatial resolutions do not change throughout their volumes.

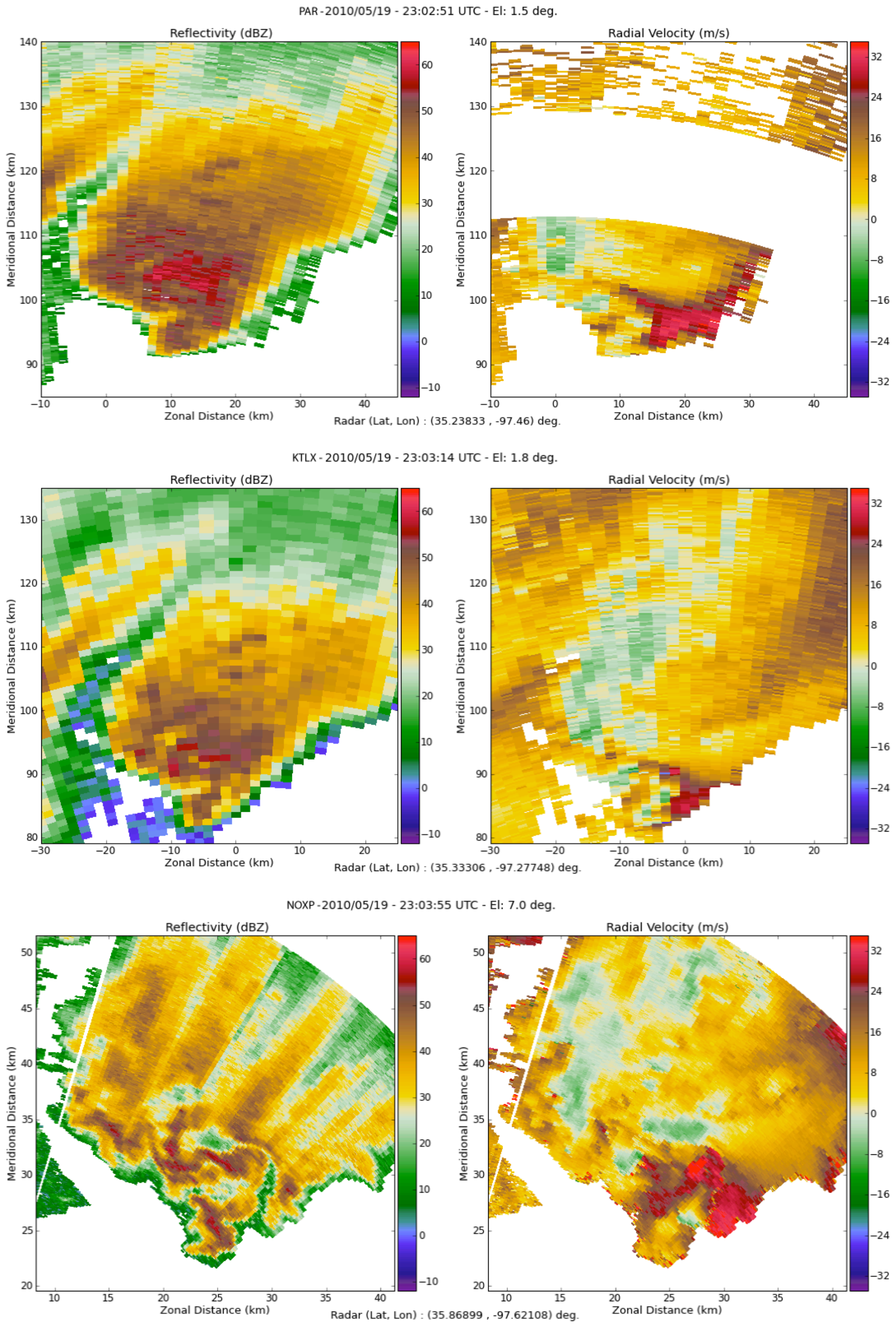

Figure 5 – Same as Fig. 3 but at KTLX's 1.8° elevation. As noted in Fig. 3, NOXP's signal is still attenuated down certain radials. The beam is much higher above ground level due to the longer range and higher elevation angle. The reduction of attenuation is attributed to the dominant hydrometeor type in the region being mostly composed of ice crystals. As noted in Fig. 4, PAR and NOXP's spatial resolution exceeds the 88D's legacy resolution.

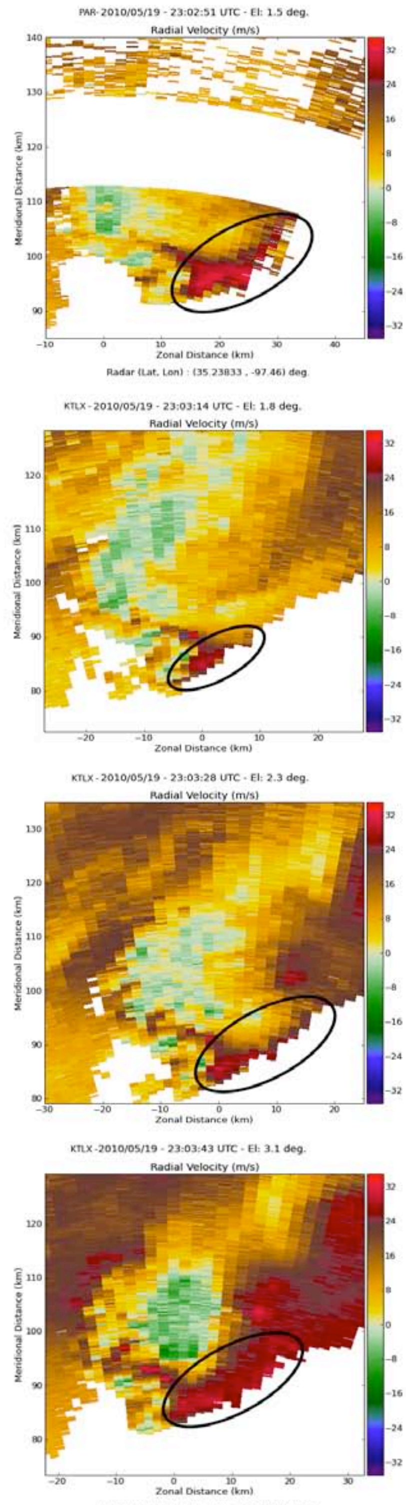

Figure 6 – Illustration of the vertical side lobe problem with the PAR in radial velocity data. The ellipse denotes the notable region in question. In the bottom three panels are KTLX elevations, with 1.8° coinciding with PAR's 1.5° elevation. The KTLX 2.3° and 3.1° elevation scans indicate the strong radial velocities (denoted by the ellipses) observed at the lower elevation PAR scan.

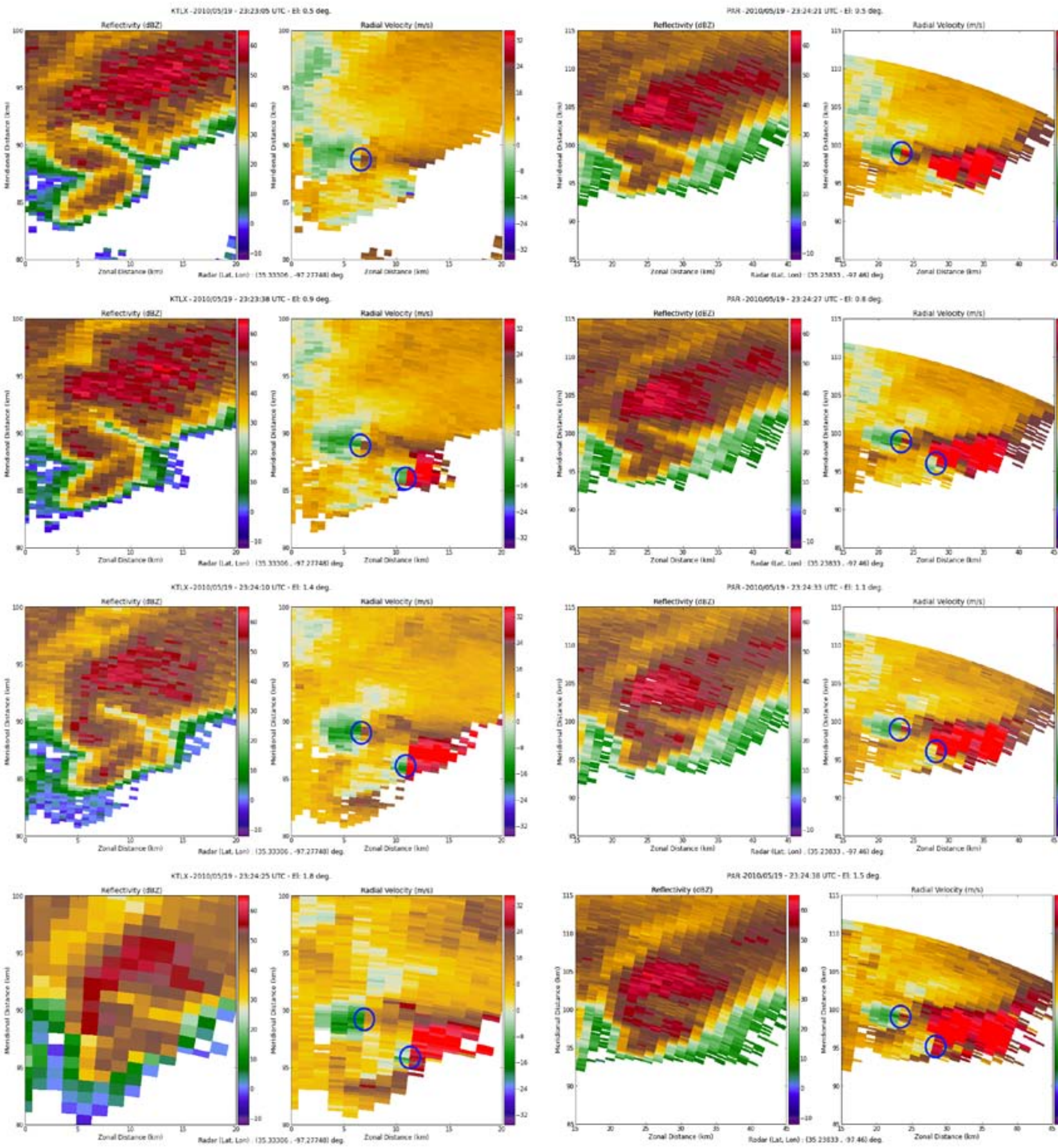

Figure 7 – KTLX (left side of image) and PAR (right side of image) Reflectivity (left side of each panel) and Radial Velocity (right side of each panel). KTLX data are taken during the 2323:05 volume scan, and the PAR data are taken during the 2323:41 volume scan. The elevation angles of KTLX (from top to bottom) are 0.5°, 0.9°, 1.3°, and 1.8°, respectively. The elevation angles of PAR (from top to bottom) are 0.51°, 0.81°, 1.15°, and 1.54°, respectively. The annotated blue circles in the Radial Velocity data indicate two regions of stronger cyclonic shear. The upper-left blue circle on the left side of both PAR and KTLX velocity scans is associated with the Lake Carl Blackwell tornado; the lower-right blue circle is associated with a newly developed mesocyclone that was part of the supercell cyclic process. Side lobe contamination in the PAR Radial Velocity data is apparent in all four scans.

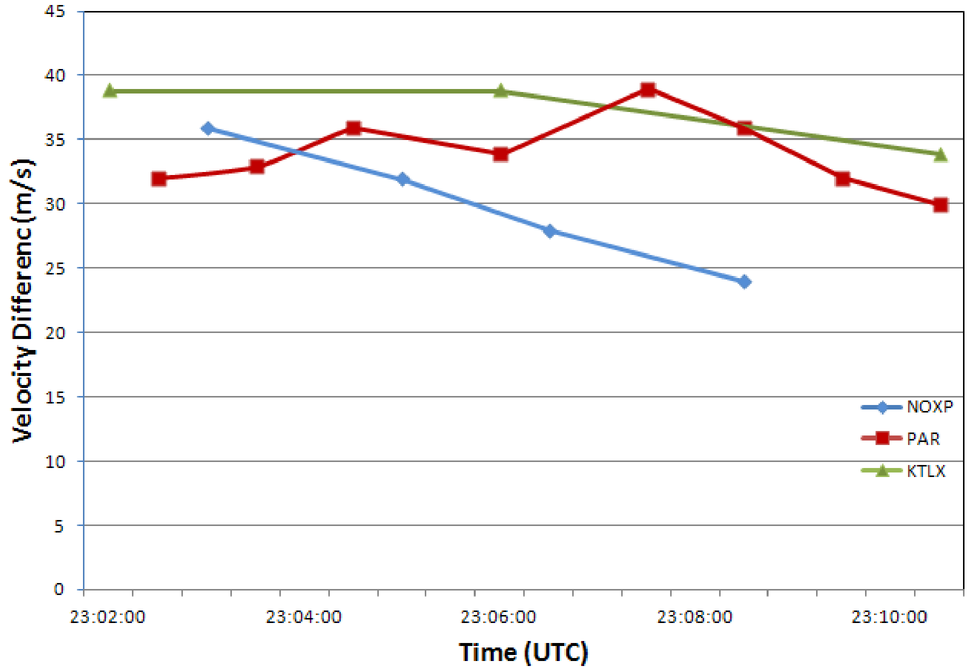

Figure 8 – Velocity Difference/Time plot for the Kingfisher Mesocyclone

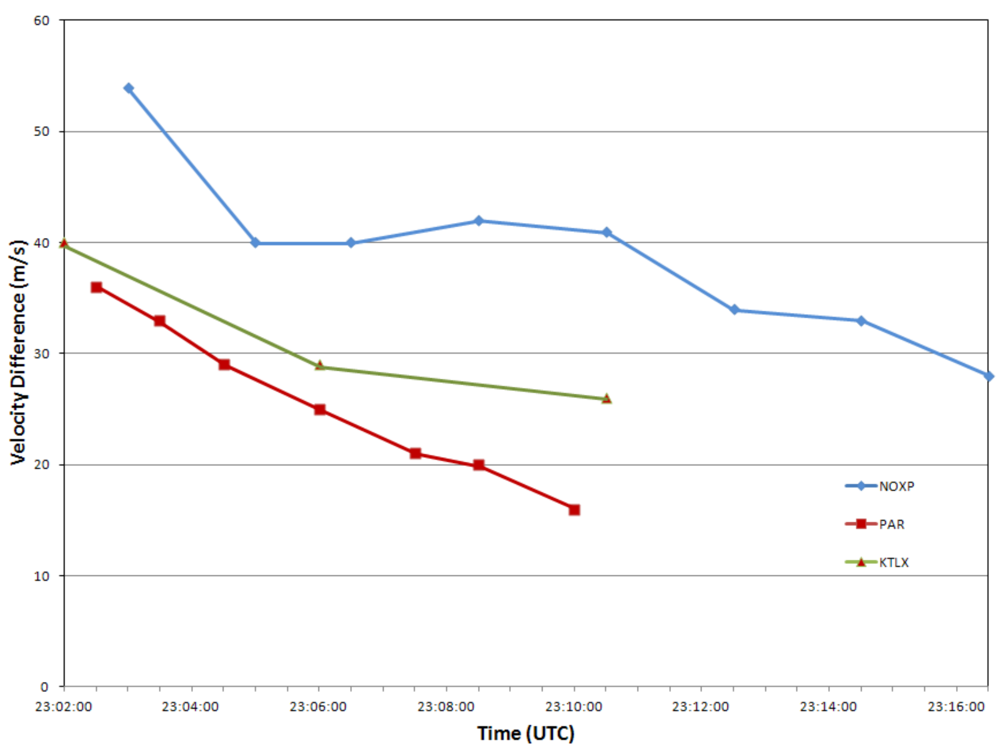

Figure 9 – Velocity Difference/Time Plot for the Orlando Mesocyclone

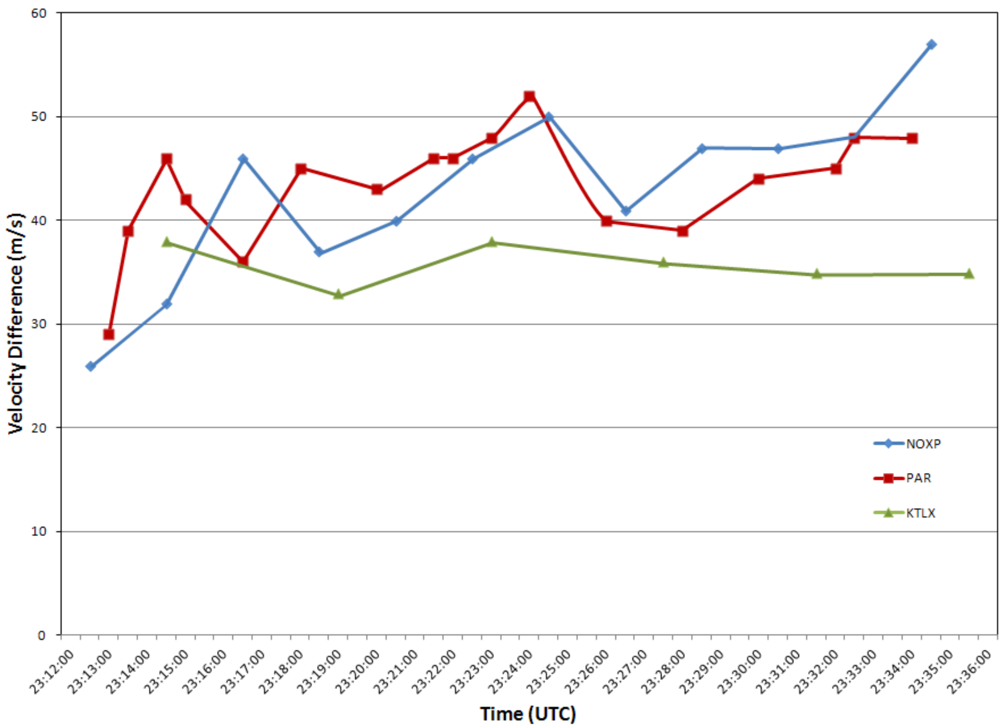

Figure 10 – Velocity Difference/Time plot for the Lake Carl Blackwell Mesocyclone

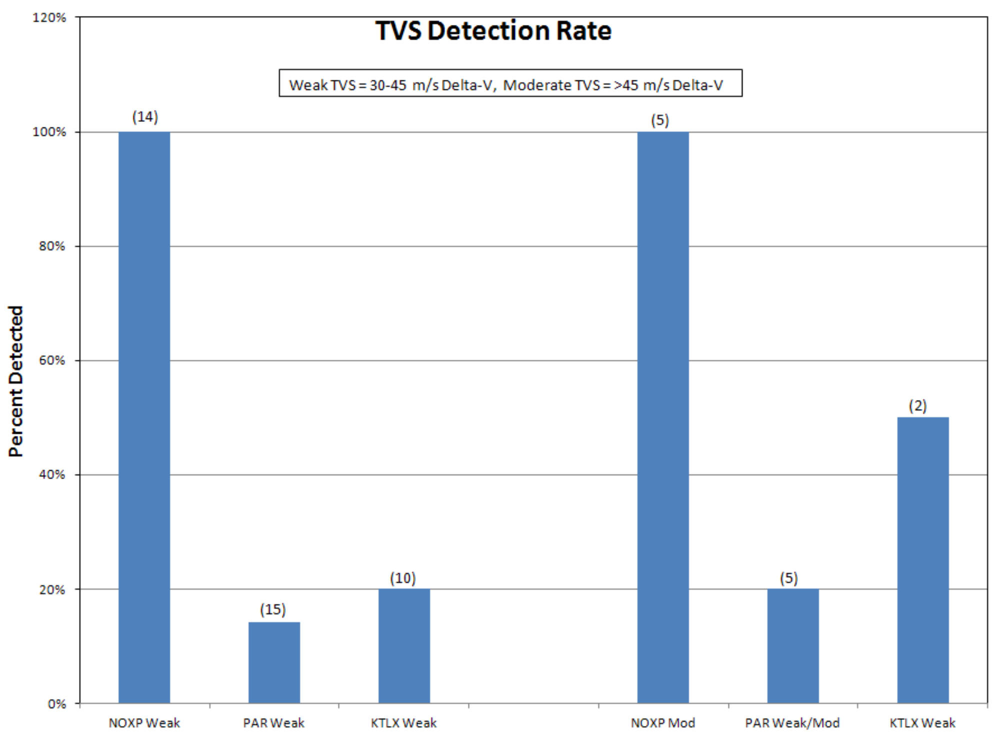

Figure 11 – Percentage of TVS detections for PAR and KTLX compared to NOXP for weak and moderate TVSs.